Resonant Excitation-Induced Nonlinear Mode Coupling in a Microcantilever Resonator

Yanyan Li,[1] Wenyao Luo,[1] Zhixin Zhao,[1] and Duo Liu[1,2,*]

[1] *Institute of Novel Semiconductors, State Key Laboratory of Crystal Materials, Shandong University, 27 South Shanda Road, Jinan, Shandong 250100, People's Republic of China*

[2] *Jinan Institute of Quantum Technology, Jinan, Shandong 250101, People's Republic of China*

(Received 13 October 2021; revised 17 April 2022; accepted 19 April 2022; published 10 May 2022)

The nonlinear dynamics of microelectromechanical resonators has recently garnered significant attention for their potential use in high-precision detection and information processing. In this paper, we report resonant excitation as a powerful tool for generating nonlinear mode coupling in a cantilever microresonator. It is discovered that resonant driving at its second flexural mode f_2 under moderate driving amplitude gives rise to blue and red sidebands due to mode coupling between the fundamental mode and the second flexural mode. Detuning the driving frequency enables a continuous shift in the frequencies of the blue and red sidebands with a frequency span of 220 Hz. Further increase in the drive amplitude at f_2 mode splitting, and broadband acoustic frequency comb with a frequency span exceeding 500 kHz. Our findings pave the way towards parametric control based on injection locking for manipulating multimode mechanical resonator systems.

DOI: 10.1103/PhysRevApplied.17.054015

I. INTRODUCTION

Mechanical resonators with high precision and excellent compatibility with various materials and IC circuits [1] have become a highly flexible platform for the development of high-performance sensors [2–6], filters [7–9], gyroscope [10], transducers [11,12], and oscillators [13–15], and as tools for fundamental scientific endeavors. Recently, the nonlinear dynamics of microresonators has been explored for their potential use in quantum state manipulation and information processing [16–18] owing to their low energy consumption and the ability to achieve efficient energy transfer and strong coupling between different modes [19–22]. Parametric excitation has become a routine technique to achieve mode coupling in a nonlinear system. Thus far, various nonlinear effects, such as mechanical sideband [23–25], injection locking [26,27], four-wave mixing [28], and parametric normal-mode splitting [29,30], have been experimentally demonstrated in mechanical microresonators. Acoustic frequency combs (AFCs) in mechanical microresonators have recently received considerable attention. AFCs, which consist of a series of equally spaced discrete frequencies, have potential applications in quantum information processing, enhanced heat or sound transport, and high-throughput, high-precision signal sensing and imaging. The previously reported AFCs mostly arise from degenerate four-wave mixing (D4WM) of two nearby modes through cubic nonlinearities [31–35]. As a result, these AFCs usually exhibit a limited number of "teeth," e.g., less than 20, as the required zero-dispersion condition is difficult to manage to be satisfied [36–38].

In this work, we demonstrate resonant excitation as a powerful tool for nonlinear mode coupling in a cantilever microresonator. By moderate resonant driving at the second flexural mode f_2 of the microcantilever, sidebands located at the sum and difference frequencies between the second flexural mode f_2 and the fundamental flexural mode f_1 are observed. In comparison, strong resonant driving at f_2 results in frequency combs with a frequency span across multiple modes from 0 to 500 kHz.

II. EXPERIMENTAL DETAILS

Figure 1(a) shows the measurement setup and a SEM image of the cantilever beam used in this investigation. We use a monocrystalline silicon microcantilever beam with dimensions of 450 $\times$ 50 $\times$ 2 μm^3. The cantilever is mounted on a piezoelectric disc attached on a cuboid support with a size of $2 \times 1 \times 3$ mm^3 and placed in a vacuum chamber at approximately 10^{-2} mbar at room temperature. The piezoelectric disc is made of lead zirconate titanate (PZT) ceramic ($d_{33} \sim 350$ pmV^{-1}), with a diameter of 30 mm and a thickness of 2 mm. The piezoelectric disc oscillates vertically through an alternating voltage applied through two electrodes on the top and bottom sides. A function generator (model 332200A, Agilent, USA) is used for the application of a sinusoidal ac

*liuduo@sdu.edu.cn

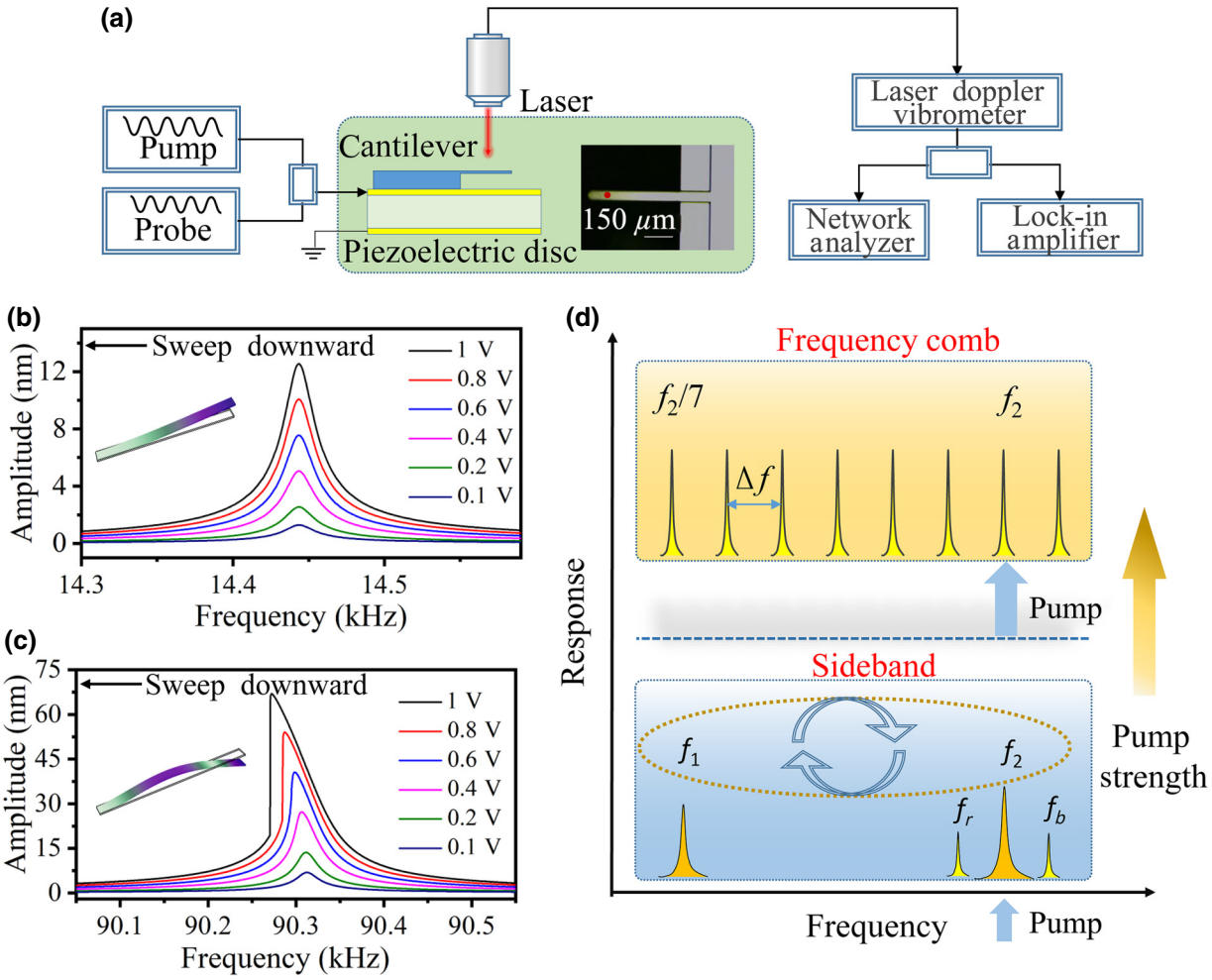

FIG. 1. (a) Measurement setup and SEM image of a microcantilever. The SEM image is mirrored as compared to the schematic drawing of the cantilever. (b), (c) Downward sweep frequency responses of the fundamental and second flexural modes under different driving voltages, respectively. The insets are the corresponding mode shapes of the two modes. (d) Schematic illustration of the coupled system. A moderate driving power at f_2 gives rise to a red (f_r) sideband and a blue (f_b) sideband owing to the coupled interaction between f_1 and f_2. A strong driving power creates frequency combs because of higher-order nonlinear interactions.

pump at frequency f_{pump} and voltage V_{pump}. The cantilever motion is monitored using a Doppler vibrometer (model OFV-5000/534, Polytec, Germany) equipped with a high-precision low-noise lock-in amplifier (model MFLI5M, Zurich Instruments, Switzerland) and a network analyzer (E5061B, Agilent, USA). We pick up a point with the largest displacement on the microcantilever for the detection of vibrational signals, as marked by a red dot on the SEM image of Fig. 1(a). The motion of the cantilever beam consists of multiple resonant modes. Herein, the fundamental and second flexural modes of the cantilever beam are the modes of interest.

III. RESULTS AND DISCUSSIONS

Figures 1(b) and 1(c) show the downward sweep frequency responses of the fundamental and second flexural modes, respectively, under different driving amplitudes. A finite-element-method simulation verifies that the two modes have different mode shapes (see the insets). The resonance frequencies and Q factors of the two modes are determined by Lorentzian fitting of the experimental data obtained at a small probe amplitude $V_{\text{probe}} = 0.1$ V. The resonance frequencies are $f_1 = 14.44$ kHz and $f_2 = 90.31$ kHz. The ratio $f_2/f_1 = 6.25$ is close to the theoretical value of 6.27 for a homogeneous cantilevered Euler-Bernoulli beam [39]. The corresponding Q factors of the two modes are $Q_1 = 365.6$ and $Q_2 = 1913.0$. In particular, as shown in Fig. 1(c), the second flexural mode exhibits a softening Duffing nonlinearity upon increasing the probe voltage V_{probe} from 0.4 to 1 V (peak voltages).

The resonant excitation gives rise to a nonlinear channel formed by interactions between different harmonics of the microresonator and the piezoelectric disc for energy

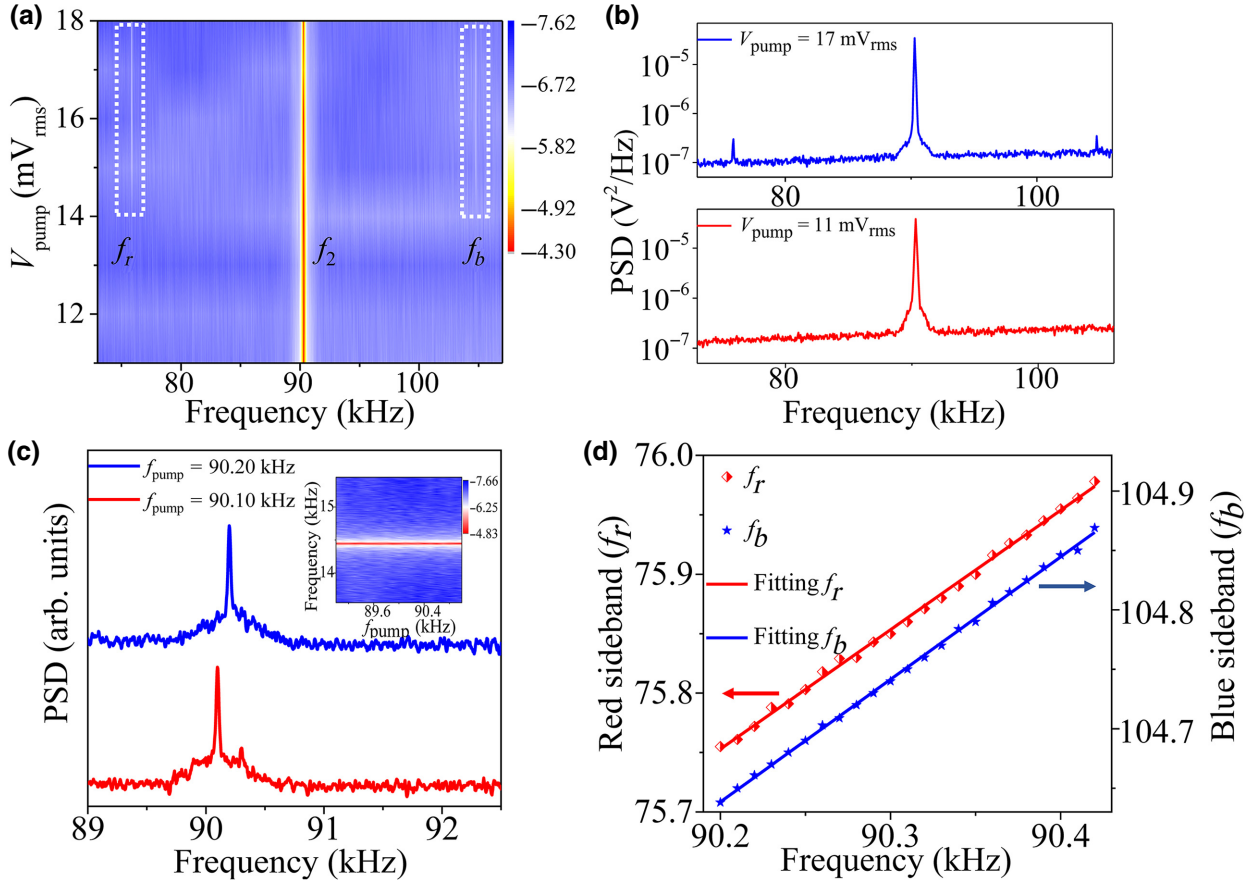

FIG. 2. (a) Logarithmic (base 10) scale contour plot of the PSD spectra of the cantilever beam upon increasing the drive voltage V_{pump} at f_2. The color bar indicates the amplitude in dB. (b) Two typical line profiles extracted from (a) without (bottom) and with (top) the sidebands at f_r and f_b. (c) The PSD spectra measured by detuning the drive frequency f_{pump} at V_{pump}= 17 mV$_{rms}$. This inset shows that the first flexural mode at f_1 remains stable as the f_{pump} changes. The color bar indicates the amplitude in dB. (d) Drive frequency f_{pump} varying from 90.20 to 90.40 kHz in a step of 0.01 kHz results in a linear dependent variation of the red and blue sidebands, as confirmed by the least-squares fittings (solid lines).

transfer between the coupled modes. To demonstrate the nonlinear behavior of the system under resonant driving, we apply a sinusoidal excitation signal at $f_{pump}=f_2$ of different driving amplitudes to the microcantilever. The signal at f_1 arises from thermal noise [40]. As schematically depicted in Fig. 1(d), we first apply a moderate driving excitation f_{pump} in the second flexural mode f_2. We measure the power spectral density (PSD) of the cantilevered beam by varying the driving amplitude V_{pump} from 11 to 18 mV$_{rms}$ (root-mean-square voltage). Figure 2(a) shows the PSD spectra around f_2, detected using the autocorrelation technique [41]. As shown in Fig. 2(a), increasing the driving amplitude at f_2 creates two sidebands at the difference f_2-f_1 and the sum f_1+f_2, which clearly indicates mode coupling between the two modes at f_1 and f_2. The frequency difference f_2-f_1 (75.87 kHz) and the sum f_1+f_2 (104.75 kHz) are denoted as f_r and f_b, respectively. Figure 2(b) shows two typical line profiles extracted from Fig. 2(a) before and after the formation of the two sidebands. The underlying mechanism can be understood as follows. The generation of sidebands around f_2 arises from modulation of the mode f_2 by the first mode at f_1 as a function of time [42].

For a resonator, injection locking involves parametric driving at a frequency close to its natural resonance frequency. Once the drive amplitude exceeds a threshold value, the resonator can be locked to the drive in frequency and phase. We then measure the PSD spectra around f_2 by varying the drive frequency f_{pump} from 90.1 to 90.2 kHz at a constant drive voltage V_{pump}= 17 mV$_{rms}$. As shown in Fig. 2(c), increasing f_{pump} from 90.1 to 90.2 kHz resulted in injection locking of the second flexural mode by the driving signals [43]. This inset of Fig. 2(c) shows that the mode at f_1 remains stable as the drive frequency f_{pump} changes. Note that the first flexural mode at f_1 is maintained at a constant frequency when the f_2 mode

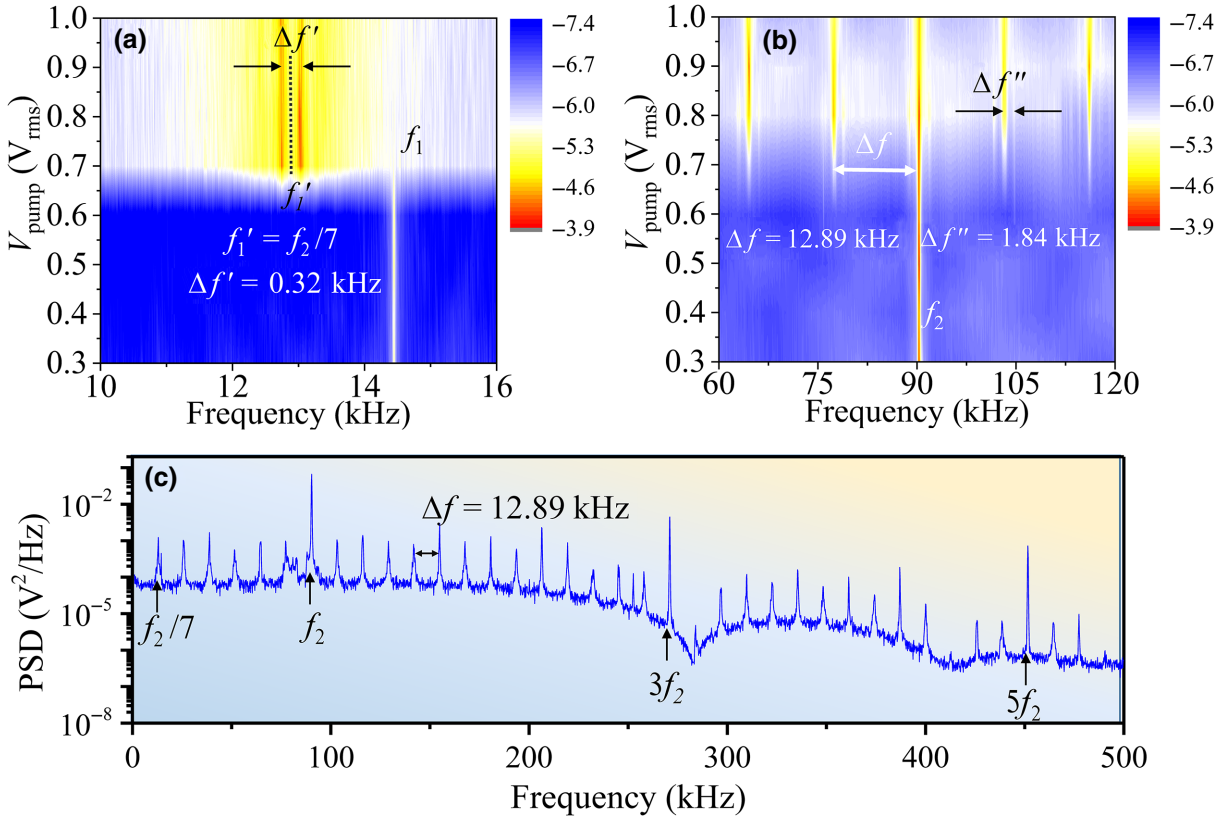

FIG. 3. When the drive frequency f_{pump} 90.31 kHz is equal to f_2, the drive voltage V_{pump} gradually increases from 0.3 to 1 V_{rms}. (a), (b) Logarithmic (base 10) scale contour plots of the first and second flexural mode PSD responses as functions of the V_{pump}. The color bar indicates the amplitude in dB. With the V_{pump} increasing, the parametric coupling is enhanced. The red lines are displayed under a strong resonant drive with a mode splitting of 0.32 kHz. (c) Extracted PSD spectra from (b) for a strong parametric drive power $V_{pump} = 0.7$ V_{rms} at $f_{pump} = 90.31$ kHz is equal to f_2.

is driven at different frequencies. The maximum locking range [26,27,44] in this case can be written as

$$\Delta\delta = \frac{f_2}{2Q_2} \times \frac{A_{inj}}{A_{osc}} \times \frac{1}{\sqrt{1-(A_{inj}/A_{osc})^2}}. \quad (1)$$

Thus, it depends on the amplitude ratio of the injection-locked oscillation A_{inj} and the original resonant oscillation A_{osc} at f_2 and the ratio of f_2 to the mechanical quality factor Q_2.

The continuous frequency shift of the sidebands realized by the injection locking is demonstrated by measuring the sideband frequencies as a function of f_{pump}. The red and blue curves in Fig. 2(d) correspond to the red sideband f_r and the blue sideband f_b frequency curves as the drive frequency f_{pump} is increased. As shown in Fig. 2(d), by changing f_{pump}, we observe that the frequency shifts of the two sidebands exactly track the frequency shift of the drive signals with a frequency span of 220 Hz. However, it should be noted that external driving of a damped resonator could also result in the above observations. The ability to tune the sidebands continuously makes this system an interesting candidate for high-precision signal detection or filtering applications through sideband modulation to improve signal-to-noise ratio, with potentials to be integrated into atomic force microscopy (AFM).

Second, we apply a stronger drive at the second flexural mode f_2. Figure 3 is a power spectra obtained by frequency scan at zero voltage through thermal noise excitation. Figures 3(a) and 3(b) depict the response of the microcantilever to a gradual increase in the drive voltage V_{pump} from 0.3 to 1 V_{rms} at $f_{pump} = f_2 = 90.31$ kHz. Notably, when the drive voltage reaches 0.7 V_{rms}, two new narrow peaks separated by $\Delta f' = 0.32$ kHz suddenly appear at 12.73 and 13.05 kHz. The center frequency f_1' between the two peaks is located at 12.89 kHz with a frequency ratio $f_2/f_1' = 7.006$, suggesting the occurrence of (1:7) internal resonance (IR). The frequency ratio remains at 7.006 and deviates slightly from 7, which could be related to frequency pulling induced by mode coupling and/or geometric uncertainties [44]. The mode at f_1' undergoes a mode splitting and is divided into two satellites at 12.73 and 13.05 kHz with a frequency separation $\Delta f' = 0.32$ kHz, as depicted by the red lines in

Fig. 3(a) [45]. From Fig. 3(b), we also observe alternative satellites with a separation $\Delta f'' = 1.84$ kHz. From the frequencies extracted from the experimental data, we find that $f_1' \approx 7\Delta f''$.

Furthermore, we observe AFCs upon strong driving, and the frequency combs show a well-defined interval $\Delta f = f_1' = 12.89$ kHz. The teeth of the combs extend over a frequency range of approximately 500 kHz. The generation of the frequency combs can be attributed to the frequency mixing of the second flexural mode and the IR-induced injection-locked f_1' mode. Energy and momentum conservation places stringent conditions on the formation of AFCs. To obtain broadband AFCs, zero dispersion in a broad frequency range needs to be satisfied, analog to optical frequency combs [36,37]. Spring constant (k) increases as the frequency increases, suggesting a positive dispersion for k. In contrast, the geometric dispersion for a microcantilever is negative when it is strongly driven, resulting in Duffing-like softening [46]. Therefore, the broad frequency span can be attributed to the compensation of the intrinsic spring dispersion of the microresonator by geometric nonlinearity induced by resonant excitation. In addition, as shown in Fig. 3(c), we observe that the modes at f_2, $3f_2$, and $5f_2$ with large amplitudes are significantly more prominent than other modes.

There are abundant nonlinear behaviors in a nonlinear system with coupled modes when forcedly pumped at one of the resonant modes. In this study, the signal f_{pump} is applied at f_2, which induced large anharmonic deformations of both the piezoelectric disc and the cantilever beam. For a symmetric anharmonic oscillator, the restoring force can be expressed as follows:

$$F(x_2) = -\omega_2^2 x_2 - \sum_{j=1}^{N} a_j x_2^{2j+1}, \tag{2}$$

where x_2 is a displacement of the system and a_j are the nonlinear coefficients. The dynamic behaviors of the system can be expressed as follows [47–51]:

$$\ddot{x}_1 + \gamma_1 \dot{x}_1 + \omega_1^2 x_1 + \alpha_{12} x_1 x_2 = 0, \tag{3}$$

$$\ddot{x}_2 + \gamma_2 \dot{x}_2 + \omega_2^2 x_2 + \sum_{j=1}^{N} a_j x_2^{2j+1} + \alpha_{21} x_1 x_2 = \sum_{n=1}^{\infty} \mathrm{A}_n \sin\ n\omega_p t, \tag{4}$$

where x_i denotes a displacement; γ_i is the dissipation rate; ω_i is the natural frequency; subscript $i = 1, 2$ denotes the modes f_1 and f_2, respectively; and α_{12} and α_{21} denote the quadratic coupling coefficients. The right-hand side of Eq. (4) represents a driving force possessing an infinite number of harmonics characterized with driving frequencies $n\omega_p$ and amplitudes A_n, where n is an integer. Alternatively, Eq. (4) can be rewritten as

$$\ddot{x}_2 + \omega_2^2 x_2 + \alpha_{21} x_1 x_2 = \mathrm{f}(\omega_p t, x_2, \dot{x}_2), \tag{5}$$

which can be evaluated by using the method of averaging based on perturbation [47,48,52] by introducing $x_2 = \beta \cos(\omega_2 t + \phi)$ into the $\mathrm{f}(\omega_p t, x_2, \dot{x}_2)$. The result is

$$\ddot{x}_2 + \omega_2^2 x_2 + \alpha_{21} x_1 x_2 = \mathrm{f}(\omega_p t, \beta \cos(\omega_2 t + \phi), -\beta\omega_2 \sin(\omega_2 t + \phi)). \tag{6}$$

Subsequently, the Taylor series expansion of f $(\omega_p t, \beta \cos(\omega_2 t + \phi),\ -\beta\omega_2 \sin(\omega_2 t + \phi))$ will include $\sin(n\omega_p + m\omega_2)t$ and $\cos(n\omega_p + m\omega_2)t$ in the expansion, which indicates that there are harmonic components with combined frequency at $n\omega_p + m\omega_2$ in the interference force. In other words, when $n\omega_p + m\omega_2 = \omega_2$, Eq. (5) has solutions, and resonance occurs at $p\omega_2/q$, where p and q are integers [53–56].

We then show that the interval of the frequency combs can be finely tuned through frequency detuning of the drive frequency f_{pump} around the mode f_2. In the experiments, f_{pump} is varied from 90.20 to 90.40 kHz in a step of 0.01 kHz for a strong parametric drive voltage $V_{\text{pump}} = 1$ V_{rms}. AFCs with different comb densities and frequency intervals Δf are obtained, as confirmed in Fig. 4. Notably, mode locking occurs when the frequency interval $\Delta f = f_1'$ is a rational multiple of that of the mode f_2, pf_2/q. In our experiments, rational multiples we observe include 1/3, 1/4, 1/5, 1/6, 1/7, 1/8, 1/9, 1/11, 1/12, 1/13, and 1/14. Note that a similar phenomenon, named Devil's staircase, had been reported on the shunted Josephson junction in the 1970s by Belykh and Pedersen [57,58], which is closely linked to "Arnold tongues" [59–62] that occurs when two or more nonlinear oscillators are coupled and their phases are locked (synchronized) to a rational multiple. Arnold tongues appear most frequently between oscillators, especially when one oscillator drives another, but not the other way around. This situation is similar to our case where the microcantilever resonator is driven by the piezoelectric disc. In addition, mechanical microresonators have tremendous potentials to be used as high-frequency clocks that demands high-frequency stability [63,64]. However, as the dimensions of microresonators shrink, they become vulnerable to external interferences [65], such that developing technologies that support multichannel frequency stabilization is necessary [14,66–68]. We show that the AFCs demonstrated in this work can be used as a multichannel frequency stabilizer that can effectively resist laser-induced photothermal effect [69–71]. Details are given in Note S1 within the Supplemental Material [72].

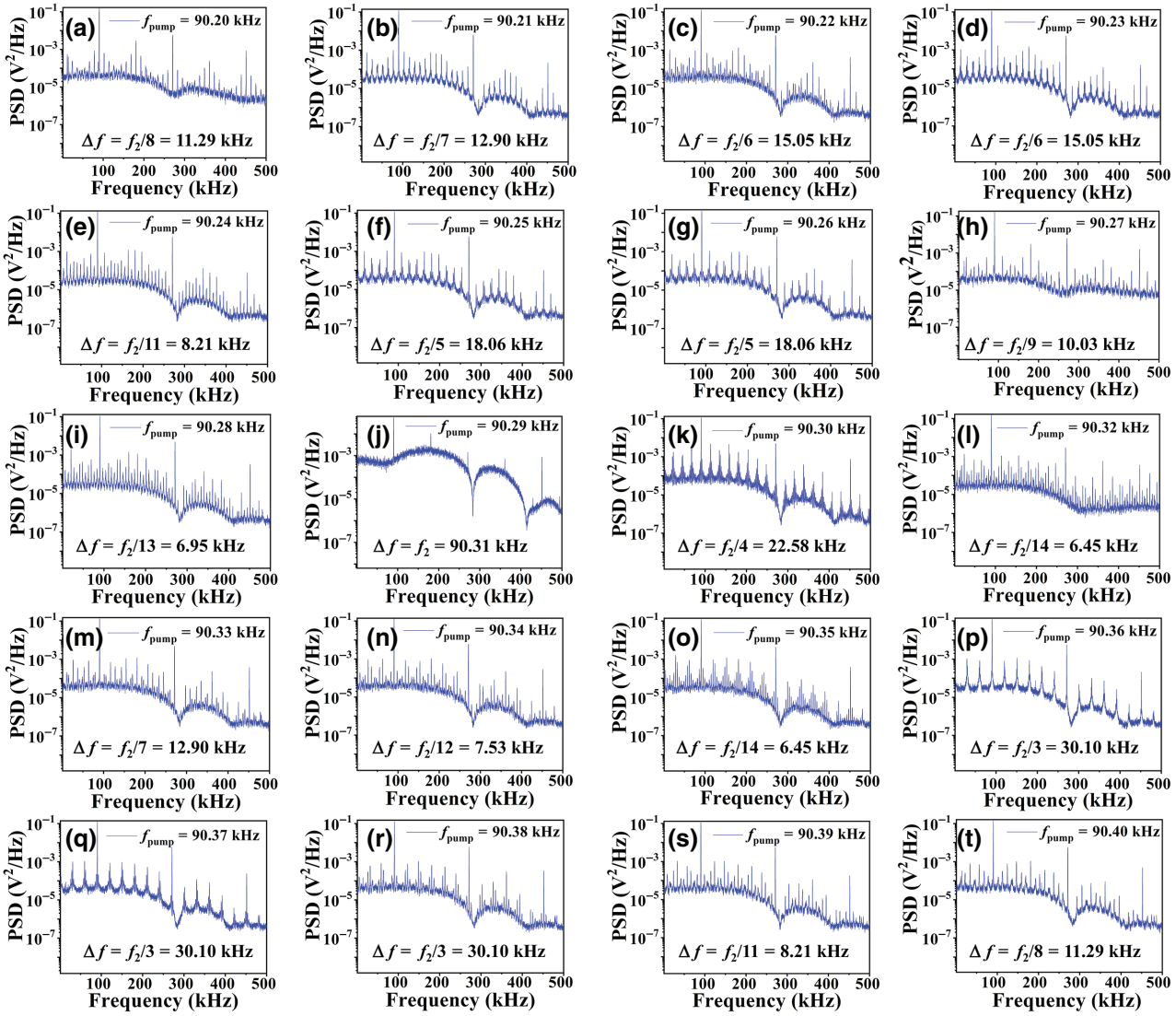

FIG. 4. (a)–(t) Logarithmic (base 10) scale plots of the PSD spectra of the microcantilever under parametric excitation by varying the drive frequency f_{pump} from 90.20 to 90.40 kHz in a step of 0.01 kHz at a fixed drive voltage V_{pump}= 1 V_{rms}. A fine tune of the frequency interval Δf for the AFCs is obtained.

Notably, as a symmetric anharmonic oscillator has only odd harmonics, the amplitudes at f_2, $3f_2$, and $5f_2$ are more prominent than those of other modes [73]. In addition, newly formed modes at $f_1' = pf_2/q$ appear owing to coupled nonlinear responses induced by resonant excitation. Subsequently, f_1' and f_2 undergo second-order nonlinear coupling to generate mutually coupled sidebands equally spaced around f_2. If the sidebands are sufficiently intense, they can further interact with high-order harmonics of f_2 and ultimately generate frequency combs with a frequency interval of f_1' and a span of 500 kHz. In other words, the frequency combs is generated because f_1' and f_2 produce a cascade second-order nonlinear process [36,74].

IV. CONCLUSION

In this study, we demonstrate resonant excitation as a tool that can manipulate nonlinear mode coupling in a cantilever beam microresonator. For small amplitude excitation, the microcantilever shows two flexural modes at f_1= 14.44 kHz and f_2 = 90.31 kHz. As we increase the drive amplitude to exceed a moderate threshold, the spectrum near f_2 shows two sidebands at the frequencies $f_2 - f_1$ and $f_2 + f_1$. A slight detuning of the drive frequency resulted in a continuous frequency shift of the sidebands for a frequency span of 220 Hz. As the drive amplitude grows further and exceeds a relatively high threshold, AFCs across multiple modes are observed.

A frequency detuning of the drive results in AFCs with different frequency intervals $\Delta f = pf_2/q$. The presented method opens up a path towards parametric control based on injection locking for the controlled manipulation of multimode mechanical resonator systems.

ACKNOWLEDGMENTS

The authors acknowledge the National Science Foundation of China (NSFC) (Grants No. 52172296 and No. 51472143), the National Key R&D Program of China (NKRD) (Grant No. 2017YFB0405403), and the Initiative in Quantum Science of Shandong Provincial Natural Science Foundation (Grant No. ZR2020LLZ005) for financial support.

[1] J. P. Mathew, R. N. Patel, A. Borah, R. Vijay, and M. M. Deshmukh, Dynamical strong coupling and parametric amplification of mechanical modes of graphene drums, Nat. Nanotechnol. **11**, 747 (2016).

[2] S. Dominguez-Medina and S. Fostner, Neutral mass spectrometry of virus capsids above 100 megadaltons with nanomechanical resonators, Science **362**, 918 (2018).

[3] C. Zhao, X. Zhou, M. Pandit, G. Sobreviela, S. Du, X. Zou, and A. Seshia, Toward High-Resolution Inertial Sensors Employing Parametric Modulation in Coupled Micromechanical Resonators, Phys. Rev. Appl. **12**, 044005 (2019).

[4] Y. T. Yang, C. Callegari, X. L. Feng, K. L. Ekinci, and M. L. Roukes, Zeptogram-scale nanomechanical mass sensing, Nano Lett. **6**, 583 (2006).

[5] R. S. Decca, D. López, H. B. Chan, E. Fischbach, D. E. Krause, and C. R. Jamell, Constraining New Forces in the Casimir Regime using the Isoelectronic Technique, Phys. Rev. Lett. **94**, 240401 (2005).

[6] D. Rugar, R. Budakian, H. J. Mamin, and B. W. Chui, Single spin detection by magnetic resonance force microscopy, Nature **430**, 329 (2004).

[7] A. H. Safavi-Naeini, T. P. Alegre, J. Chan, M. Eichenfield, M. Winger, Q. Lin, J. T. Hill, D. E. Chang, and O. Painter, Electromagnetically induced transparency and slow light with optomechanics, Nature **472**, 69 (2011).

[8] K. Wang, A. C. Wong, and C. C. Nguyen, VHF free-free beam high-Q micromechanical resonators, J. Microelectromech. Syst. **9**, 347 (2000).

[9] J. R. Clark, W. T. Hsu, M. A. Abdelmoneum, and C. C. Nguyen, High-Q UHF micro-mechanical radial-contour mode disk resonators, J. Microelectromech. Syst. **14**, 1298 (2005).

[10] K. Liu, W. Zhang, W. Chen, K. Li, F. Dai, F. Cui, X. Wu, G. Ma, and Q. Xiao, The development of micro-gyroscope technology, J. Micromech. Microeng. **19**, 113001 (2009).

[11] J. Moser, J. Güttinger, A. Eichler, M. J. Esplandiu, D. E. Liu, M. I. Dykman, and A. Bachtold, Ultrasensitive force detection with a nanotube mechanical resonator, Nat. Nanotechnol. **8**, 493 (2013).

[12] L. Yan, W. Pang, E. S. Kim, and W. C. Tang, Piezoelectrically transduced low-im-pedance microelectromechanical resonators, Appl. Phys. Lett. **87**, 154103 (2005).

[13] K. Hammerer, M. Wallquist, C. Genes, M. Ludwig, F. Marquardt, P. Treutlein, and H. J. Kimble, Strong Coupling of a Mechanical Oscillator and a Single Atom, Phys. Rev. Lett. **103**, 063005 (2009).

[14] D. Antonio, D. H. Zanette, and D. López, Frequency stabilization in nonlinear micro-mechanical oscillators, Nat. Commun. **3**, 1 (2012).

[15] M. Zalalutdinov, K. L. Aubin, M. Pandey, A. T. Zehnder, R. H. Rand, H. G. Craighead, and J. M. Parpia, Frequency entrainment for micromechanical oscillator, Appl. Phys. Lett. **83**, 3281 (2003).

[16] A. D. O'Connell, M. Hofheinz, M. Ansmann, R. C. Bialczak, M. Lenander, E. Lucero, M. Neeley, D. Sank, H. Wang, and M. Weides, Quantum ground state and single-phonon control of a mechanical resonator, Nature **464**, 697 (2010).

[17] J. D. Teufel, T. Donner, D. Li, J. W. Harlow, M. S. Allman, K. Cicak, and R. W. Simmonds, Sideband cooling of micromechanical motion to the quantum ground state, Nature **475**, 359 (2011).

[18] I. Wilson-Rae, P. Zoller, and A. Imamoáÿąlu, Laser Cooling of a Nanomechanical Resonator Mode to its Quantum Ground State, Phys. Rev. Lett. **92**, 075507 (2004).

[19] S. S. Verbridge, R. Ilic, H. G. Craighead, and J. M. Parpia, Size and frequency dependent gas damping of nanomechanical resonators, Appl. Phys. Lett. **93**, 013101 (2008).

[20] J. S. Aldridge and A. N. Cleland, Noise-Enabled Precision Measurements of a Duffing Nanomechanical Resonator, Phys. Rev. Lett. **94**, 156403 (2005).

[21] L. S. Cao, D. X. Qi, R. W. Peng, M. Wang, and P. Schmelcher, Phononic Frequency Combs Through Nonlinear Resonances, Phys. Rev. Lett. **112**, 075505 (2014).

[22] W. Luo, N. Gao, and D. Liu, Multimode nonlinear coupling induced by internal resonance in a microcantilever resonator, Nano Lett. **21**, 1062 (2021).

[23] A. Schliesser, R. Rivière, G. Anetsberger, O. Arcizet, and T. J. Kippenberg, Resolved-sideband cooling of a micromechanical oscillator, Nat. Phys. **4**, 415 (2008).

[24] I. Mahboob, K. Nishiguchi, H. Okamoto, and H. Yamaguchi, Phonon-cavity electro-mechanics, Nat. Phys. **8**, 387 (2012).

[25] W. J. Venstra, H. J. R. Westra, and H. S. J. van der Zant, Q-factor control of a micro-cantilever by mechanical sideband excitation, Appl. Phys. Lett. **99**, 151904 (2011).

[26] R. Adler, A study of locking phenomena in oscillators, Proc. IRE **34**, 351 (1946).

[27] K. Kurokawa, Injection-locking of solid state microwave oscillators, Proc. IEEE **61**, 1386 (1973).

[28] D. N. Puzyrev and D. V. Skryabin, Finesse and four-wave mixing in microresonators, Phys. Rev. A **103**, 013508 (2021).

[29] S. Gröblacher, K. Hammerer, M. R. Vanner, and M. Aspelmeyer, Observation of strong coupling between a micromechanical resonator and an optical cavity field, Nature **460**, 724 (2009).

[30] J. D. Teufel, D. Li, M. S. Allman, K. Cicak, A. J. Sirois, J. D. Whittaker, and R. W. Simmonds, Circuit cavity

electromechanics in the strong-coupling regime, Nature **471**, 204 (2011).
[31] A. Ganesan, C. Do, and A. Seshia, Observation of three-mode parametric instability in a micromechanical resonator, Appl. Phys. Lett. **109**, 193501 (2016).
[32] A. Ganesan, C. Do, and A. Seshia, Phononic Frequency Comb via Intrinsic Three-Wave Mixing, Phys. Rev. Lett. **118**, 033903 (2017).
[33] A. Ganesan, C. Do, and A. Seshia, Phononic frequency comb via three-mode para-metric resonance, Appl. Phys. Lett. **112**, 021906 (2018).
[34] M. Park and A. Ansari, in *Proc. Solid-State Sensors, Actuat. Microsyst. Workshop* (2018), p. 3.
[35] R. Singh, A. Sarkar, C. Guria, R. J. Nicholl, S. Chakraborty, K. I. Bolotin, and S. Ghosh, Giant tunable mechanical nonlinearity in graphene–silicon nitride hybrid resonator, Nano Lett. **20**, 4659 (2020).
[36] P. Del'Haye, A. Schliesser, O. Arcizet, T. Wilken, R. Holzwarth, and T. J. Kippenberg, Optical frequency comb generation from a monolithic microresonator, Nature **450**, 1214 (2007).
[37] G. Frigenti, D. Farnesi, G. Nunzi Conti, and S. Soria, Nonlinear optics in micro-spherical resonators, Micromachines **11**, 303 (2020).
[38] D. Farnesi, A. Barucci, G. C. Righini, S. Berneschi, S. Soria, and G. N. Conti, Optical Frequency Conversion in Silica-Whispering-Gallery-Mode Microspherical Resonators, Phys. Rev. Lett. **112**, 093901 (2014).
[39] P. J. P. Gonçalves, M. J. Brennan, and S. J. Elliott, Numerical evaluation of high-order modes of vibration in uniform Euler–Bernoulli beams, J. Sound Vib. **301**, 1035 (2007).
[40] R. P. Saulson, Thermal noise in mechanical experiments, Phys. Rev. D **42**, 2437 (1990).
[41] R. N. Youngworth, B. B. Gallagher, and B. L. Stamper, An overview of power spectral density (PSD) calculations, Proc. SPIE **5869**, 58690U (2005).
[42] W. J. Venstra, H. J. R. Westra, and H. S. J. van der Zant, Mechanical stiffening, bistability, and bit operations in a microcantilever, Appl. Phys. Lett. **97**, 193107 (2010).
[43] Y. Wen and N. Ares, A coherent nanomechanical oscillator driven by single-electron tunneling, Nat. Phys. **16**, 75 (2020).
[44] K. L. Turner, S. A. Miller, P. G. Hartwell, N. C. MacDonald, S. H. Strogatz, and S. G. Adams, Five parametric resonances in a microelectromechanical system, Nature **396**, 149 (1998).
[45] X. Zhou, C. Zhao, D. Xiao, J. Sun, G. Sobreviela, D. D. Gerrard, Y. Chen, I. Flader, T. W. Kenny, X. Wu, and A. A. Seshia, Dynamic modulation of modal coupling in microelectromechanical gyroscopic ring resonators, Nat. Commun. **10**, 1 (2019).
[46] M. I. Hussein and R. Khajehtourian, Nonlinear Bloch waves and balance between hardening and softening dispersion, Proc. R. Soc. A **474**, 20180173 (2018).
[47] A. H. Nayfeh, *Nonlinear Oscillations* (A Wiley- Inter-Science publication, New York, 1995).
[48] Y. S. Chen, *Nonlinear Vibration* (Science and Technology Press, Tianjin, 1983).
[49] J. Szabados, D. N. Puzyrev, Y. Minet, L. Reis, K. Buse, A. Villois, and I. Breunig, Frequency Comb Generation via Cascaded Second-Order Nonlinearities in Microresonators, Phys. Rev. Lett. **124**, 203902 (2020).
[50] A. Eichler, M. del Álamo Ruiz, J. A. Plaza, and A. Bachtold, Strong Coupling between Mechanical Modes in a Nanotube Resonator, Phys. Rev. Lett. **109**, 025503 (2012).
[51] R. De Alba, F. Massel, I. R. Storch, T. S. Abhilash, A. Hui, P. L. McEuen, and J. M. Parpia, Tunable phonon-cavity coupling in graphene membranes, Nat. Nanotechnol. **11**, 741 (2016).
[52] I. A. Mitropolsky, Averaging method in non-linear mechanics, Int. J. Non Linear Mech. **2**, 69 (1967).
[53] L. D. Landau and E. M. Lifshitz, *Mechanics* (Pergamon Press pic, Oxford, 1960).
[54] Y. Jia, S. Du, and A. A. Seshia, Twenty-eight orders of parametric resonance in a micro-electromechanical device for multi-band vibration energy harvesting, Sci. Rep. **6**, 1 (2016).
[55] S. K. Choi and S. T. Noah, Mode-locking and chaos in a Jeffcott rotor with bearing clearances, J. Appl. Mech. **61**, 131 (1994).
[56] H. Haucke and R. Ecke, Mode-locking and chaos in Rayleigh-Benard convection, Phys. D **25**, 307 (1987).
[57] V. N. Belykh, N. F. Pedersen, and O. H. Soerensen, Shunted-Josephson-junction model. I. The autonomous case, Phys. Rev. B **16**, 4853 (1977).
[58] V. N. Belykh, N. F. Pedersen, and O. H. Soerensen, Shunted-Josephson-junction model. II. The nonautonomous case, Phys. Rev. B **16**, 4860 (1977).
[59] P. L. Boyland, Bifurcations of circle maps: Arnol'd tongues, bistability and rotation intervals, Commun. Math. Phys. **106**, 353 (1986).
[60] M. H. Jensen, Inducing phase-locking and chaos in cellular oscillators by modulating the driving stimuli, FEBS Lett. **586**, 1664 (2012).
[61] S. Coombes and P. C. Bressloff, Mode locking and Arnold tongues in integrate-and-fire neural oscillators, Phys. Rev. E **60**, 2086 (1999).
[62] A. Pikovsky, M. Rosenblum, and J. Kurths, A universal concept in nonlinear sciences, Self **2**, 3 (2001).
[63] B. Wang, Z. Yang, X. Zhang, and X. Yi, Vernier frequency division with dual-micro-resonator solitons, Nat. Commun. **11**, 1 (2020).
[64] S. B. Papp, K. Beha, P. Del'Haye, F. Quinlan, H. Lee, K. J. Vahala, and S. A. Diddams, Microresonator frequency comb optical clock, Optica **1**, 10 (2014).
[65] C. Chen, S. Rosenblatt, K. I. Bolotin, W. Kalb, P. Kim, I. Kymissis, H. L. Stormer, T. F. Heinz, and J. Hone, Performance of monolayer graphene nanomechanical resonators with electrical readout, Nat. Nanotechnol. **4**, 861 (2009).
[66] S. Rana, N. D. B. Le, R. Mout, K. Saha, G. Y. Tonga, R. E. S. Bain, O. R. Miranda, C. M. Rotello, and V. M. Rotello, A multichannel nanosensor for instantaneous readout of cancer drug mechanisms, Nat. Nanotechnol. **10**, 65 (2015).
[67] G. Pillai and S. S. Li, Controllable multichannel acousto-optic modulator and frequency synthesizer enabled by nonlinear MEMS resonator, Sci. Rep. **11**, 1 (2021).
[68] D. Broda, W. J. Staszewski, A. Martowicz, T. Uhl, and V. V. Silberschmidt, Modelling of nonlinear crack–wave

interactions for damage detection based on ultrasound—A review, J. Sound Vib. **333**, 1097 (2014).

[69] M. A. Green and M. J. Keevers, Optical properties of intrinsic silicon at 300 K, Prog. Photovoltaics **3**, 189 (1995).

[70] A. Masolin, P. O. Bouchard, R. Martini, and M. Bernacki, Thermo-mechanical and fracture properties in single-crystal silicon, J. Mater. Sci. **48**, 979 (2013).

[71] N. Gao, W. Luo, W. Yan, D. Zhang, and D. Liu, Continuously tuning the resonant characteristics of microcantilevers by a laser induced photothermal effect, J. Phys. D **52**, 385402 (2019).

[72] See Supplemental Material at http://link.aps.org/supplemental/10.1103/PhysRevApplied.17.054015 for the AFCs across multiple modes and its application as a multichannel frequency stabilizer.

[73] M. Misono and K. Miyakawa, Noise-induced phase locking and frequency mixing in a Schmitt-trigger inverter with delayed feedback, J. Phys. Soc. Jpn. **79**, 034801 (2010).

[74] I. Mahboob, Q. Wilmart, K. Nishiguchi, A. Fujiwara, and H. Yamaguchi, Tunable electromechanical comb generation, Appl. Phys. Lett. **100**, 113109 (2012).